International Journal of Earth Sciences (2024) 113:353–367
https://doi.org/10.1007/s00531-023-02376-5

ORIGINAL PAPER

Laevaptychi as reliable paleotemperature archives: high-resolution stable isotope compositions of Kimmeridgian (Jurassic) lamellar structured aspidoceratid lower mandibles from Zengővárkony (Mecsek Mountains, Hungary)

László Bujtor[1] · Attila Demény[2,3] · Péter Németh[2,3] · Bernadett Bajnóczi[2,3]

Received: 9 April 2023 / Accepted: 3 December 2023 / Published online: 28 January 2024

Abstract
Fieldwork provided well-preserved *Laevaptychus* sp. ex gr. *hoplisus–obliquus* specimens from the lower Kimmeridgian of Zengővárkony (Mecsek Mountains, south Hungary). This study presents the stable isotope analysis of these aptychi and control samples from brachiopods (*Nucleata* and *Pygope*) derived from the Zengővárkony section bed 3. Rarely observed structures in the upper lamellar layers of the studied laevaptychi revealed 24–32 concentric lamellae that represent primary textural features and indicate excellent preservation. After careful screening for diagenetic effects, stable oxygen isotope compositions yielded seawater temperatures between 20 and 26 °C in good agreement with earlier studies on Jurassic formations, with improved precision. Our research presents for the first time that well-preserved laevaptychi may be a reliable data source for paleoclimate and paleotemperature reconstructions.

Keywords Palaeotemperature · Aptychus · Aspidoceratid ammonites · Tisza microcontinent · Western Tethys

Introduction

The Jurassic period was characterized by a greenhouse Earth (e.g., Sellwood and Valdes 2006), although climate fluctuations have been detected (e.g., Dera et al. 2011; Colombié et al. 2018). Jurassic seawater temperatures can be determined using geochemical data, like the distribution of organic compounds yielding TEX_{86} temperatures, clumped isotope compositions of carbonate materials of marine organisms such as bivalves and belemnites (Vickers et al. 2019, 2020, 2021; Wierzbowski et al. 2018), and stable oxygen isotope compositions ($\delta^{18}O$ values) of such samples (e.g., Alberti et al. 2022a, b). Oxygen isotope thermometry is based on the temperature dependence of carbonate–water oxygen isotope fractionation (^{18}O and ^{16}O partitioning between the two compounds). Using an appropriate fractionation equation and an estimated $\delta^{18}O$ value of seawater, the seawater temperature can be calculated. Although the oxygen isotope paleothermometry method appears straightforward, it suffers from several problems. The first is selecting the appropriate equation that describes the temperature dependence of the carbonate–water oxygen isotope system for the given carbonate type. Equations were established as early as the 1950s and 1960s (McCrea 1950; O'Neil et al. 1969), after which several experimental, theoretical, and empirical equations were established (Johnston et al. 2013; Jautzy et al. 2020). For some deposits, the governing factors are so numerous and stochastic that empirical equations containing all the effects that influence stable isotope

✉ László Bujtor
bujtor.laszlo@uni-eszterhazy.hu

✉ Attila Demény
demeny.attila@csfk.org

Péter Németh
nemeth.peter@csfk.org

Bernadett Bajnóczi
bajnoczi.bernadett@csfk.org

[1] Institute of Geography and Environmental Sciences, Eszterházy Károly Catholic University, 6-8 Leányka Street, Eger 3300, Hungary

[2] HUN-REN CSFK, MTA Centre of Excellence, Konkoly Thege Miklós út 15-17., Budapest 1121, Hungary

[3] Institute for Geological and Geochemical Research, HUN-REN Research Centre for Astronomy and Earth Sciences, Budaörsi út 45, Budapest 1112, Hungary

compositions without the exact knowledge of influences can be used. The empirical fractionation relationships are calibrated using measured temperatures and compositions of recently forming carbonates to determine paleotemperatures (e.g., Tremaine et al. 2011). Another problem is that calibration with known temperature and oxygen isotope compositions of carbonate and water is not possible for extinct organisms, like Jurassic ammonites and belemnites. Vickers et al. (2020) presented an alternative approach with independent seawater temperature determination. They measured clumped isotope compositions of belemnite rostra, which yielded seawater temperatures without the need for water composition, leading them to suggest that the belemnite calcite follows the calcite-water oxygen isotope fractionation determined by Daëron et al. (2019) for extremely slowly precipitating calcites. In the absence of independent temperature data, $\delta^{18}O$ measurements of coexisting carbonate-secreting organisms (bivalves and cephalopods) can help to estimate seawater temperatures (e.g., Sadji et al. 2021; Alberti et al. 2022a, b). These temperature estimations are strengthened when similar data are obtained using different carbonate formations and equations (e.g., Anderson and Arthur (1983) for marine calcites and Daëron et al. (2019) for belemnites).

Once the appropriate carbonate-water oxygen isotope fractionation equation is selected, the next variable is the oxygen isotope composition of seawater. The climate of the Late Jurassic was characterized by high atmospheric CO_2 levels and by a monsoonal rainfall pattern (Moore et al. 1993; Weissert and Mohr 1996). Additionally, the global stable isotope composition of the ocean was slightly lower (by about –1‰, Shackleton and Kenneth 1975) than it is today (0‰). However, the $\delta^{18}O$ of –1‰ is a global mean composition, but local values may depend on latitudinal position (Alberti et al. 2020) and local effects, like evaporation (e.g., Vickers et al. 2019). Knowing details of the formation site and organisms present (paleogeography, water depth, life habitat, neritic or sessile) allows researchers to estimate the water composition.

Late-stage alterations are also very important for the interpretation of oxygen isotope compositions. Although the thermal influence that is associated with significant fluid migration can sometimes be excluded on the basis of mineralogy (e.g., aragonite preservation), textural characteristics (e.g., scanning electron microscopic analysis), and geochemistry (e.g., low Mn content and no cathodoluminescence of the calcite), re-crystallization and isotope exchange with ambient solutions may have occurred during the > 145 million years since the sediments were deposited. It is difficult to identify carbonate formation that has not been diagenetically altered. Aragonite preservation and the presence of fine primary textures may indicate good preservation, but it is still important to measure as many samples as possible and to evaluate geochemical compositions with diagenesis as a possibility.

This study presents the analyses of calcite aptychi of ammonites and brachiopod shells to determine if they preserved the primary stable isotope signals. Ammonite shell is built of aragonite and is prone to alteration, calcitization, or dissolution, and aptychi (the lower mandible of ammonites) are secreted by the organism and are composed of a more refractory calcite. In this paper, we present the results of high-resolution stable isotope analyses of aptychi that preserved fine-scale lamination, whose unaltered parts could be selected, as well as the stable isotope compositions of brachiopod shells that may be used for comparison. This study also provides reliable seawater temperature data that fit existing estimations and demonstrates the high-resolution use of aptychus analysis on *Laevaptychus* samples to acquire reliable palaeotemperature data.

Materials and methods

Materials

The aptychus samples studied in this research were collected and published by Bujtor and Albrecht (2021) and are housed in the Palaeontological Collection of the Mining and Geological Survey of Hungary, Budapest. The laevaptychi used in this research belong to *Laevaptychus* sp. ex gr. *hoplisus–obliquus*. Aptychus terminology follows Trauth (1927). The dimensions of the analysed aptychi are indicated in Table 1.

The brachiopod samples were collected and published by Bujtor and Albrecht (2022) and are housed in the Palaeontological Collection of the Mining and Geological Survey of Hungary, Budapest. The dimensions of the analysed brachiopods are in Table 2.

Methods

Petrographic analysis was conducted using a Nikon Eclipse E600 POL optical microscope on thin, polished thin sections. Scanning electron microscope analyses were performed on broken chips of aptychi and brachiopod shells using a JEOL JSM-IT700HR instrument operated at 3.0 kV acceleration voltage. Cathodoluminescence microscopic pictures were taken with a Reliotron "cold-cathode" instrument mounted on a Nikon Eclipse E600 microscope with a Nikon Coolpix 4500 digital camera and operated at 6 to 10 keV acceleration voltage.

Calcite samples were drilled from the outer surface of aptychi or along a trench on a polished surface using a 0.6 mm drill bit. The average resolution of trench drilling was about 0.1 mm. Brachiopod shell pieces of 1–2 mm in

Table 1 Dimensions of the laevaptychi samples used in this study. Biometric data are from Bujtor and Albrecht (2021)

Repository number	L	S	L_{at}	l	G	S/L	Analysed sample
J 2020.692.1	48.6	38.2	38.9	(30)	(6)	0.79	Yes
J 2020.696.1	(47)	36.8	38.3	(31)	(7)	0.78	Yes
J 2020.698.1	(52)	45.0	44.7	(29)	7.2	0.86	Yes
J 2020.701.1	52.0	38.3	38.8	34.1	3.4	0.74	Yes
J 2020.702.1	45.9	38.6	36.7	28.2	4.0	0.84	Yes

The data in parentheses refer to an estimated value due to poor preservation. Specimens J 2020.691.1, J 2020.693.1, J 2020.699.1, J 2020.743.1, and J 2020.745.1 are not measured due to fragmentary status

Table 2 Dimensions of the brachiopod samples used in this study. Biometric data are from Bujtor and Albrecht (2022)

Scientific name with repository number	L	W	T	W/L	T/L
Nucleata bouei (Zejszner 1846) J.2020.592.1	23.1	27.2	15.9	1.18	0.69
Scientific name with repository	L	W	H	vp	dp
Pygope catulloi (Pictet 1867) J.2020.593.1	43.1	41.7	22.2	(6)	(11)

The data in parentheses refer to an estimated value due to poor preservation

L length, *W* width, *T* thickness, *H* height, *vp* length of the perforation on the ventral valve, *dp* length of the perforation on surface of the dorsal valve

size were peeled off using a box cutter and were powdered for analysis. Stable carbon and oxygen isotope compositions were determined with an automated carbonate preparation device (GASBENCH II) and a Thermo Finnigan delta plus XP continuous-flow mass spectrometer at the Institute for Geological and Geochemical Research, Research Centre for Astronomy and Earth Sciences (IGGR, Budapest, Hungary). Three laboratory standards, calibrated using the NBS-18, NBS-19, and LSVEC reference materials (provided by the International Atomic Energy Agency), were used for sample standardization. The isotope compositions are expressed as $\delta^{13}C$ and $\delta^{18}O$ values (in ‰) relative to V-PDB. To test external precision, the Harding Iceland Spar (Landis 1983) sample was measured as unknown in the period of 2019 to 2023 and yielded $\delta^{13}C$ and $\delta^{18}O$ values of -4.84 ± 0.05‰ and -18.58 ± 0.06‰, respectively ($n = 92$). These values agree well with the published $\delta^{13}C$ and $\delta^{18}O$ values of –4.80 and –18.56‰, respectively (Landis 1983); as such, the differences between the measured (at IGGR) and published values indicate external accuracies.

Geological setting

The Mecsek Mountains are situated in southern Hungary (Fig. 1b). They are the northernmost unit of the Mecsek overthrust Nappe system (or Tisza Mega unit), which is considered a microplate (Vörös 1993; Csontos and Vörös 2004; Haas and Péró 2004). Detachment of this lithosphere fragment from the southern margin of the European plate began in the middle Jurassic, but it remained near the stable European plate during the younger Mesozoic (van Hinsbergen et al. 2020).

The early Jurassic rocks (Hettangian and Sinemurian Ages) of the Mecsek Mountains are characterized by shallow, coal-bearing clastic and marly sedimentation, and a thick sandstone sequence, which suggest a rapidly subsiding sedimentary basin with cyclic, short-term paleoenvironmental changes from fluvial/deltaic to swampy conditions (Ruckwied et al. 2008). The Sinemurian and Toarcian rocks are characterized by marine sedimentary rocks including black shales. This basin is the northernmost piece of a greater tectonic unit called the Tisza Mega unit (Haas and Péró 2004).

Detachment from the European plate brought remarkable changes in sedimentation, which are recorded around the Bathonian/Callovian boundary, when pelagic sedimentation occurred in the Mecsek Mountains (Galácz 1984). This phenomenon is supported by the recent tectonic results of Tari (2015). The separation ushered the area of the Mecsek Mountains into Tethyan conditions. The subsidence of this area resulted in pelagic sedimentation of typical ammonitico rosso-type, dark red, nodular marly limestones (Raucsik in Főzy 2012), which were the most characteristic Middle Jurassic formation in the Mecsek Mountains (Óbánya Limestone Fm.). Later, this pelagic limestone sedimentation continued into the late Middle and the entire Late Jurassic. The Bathonian, Oxfordian, and the early Kimmeridgian Ages are characterized by ammonitico rosso-type sedimentation;

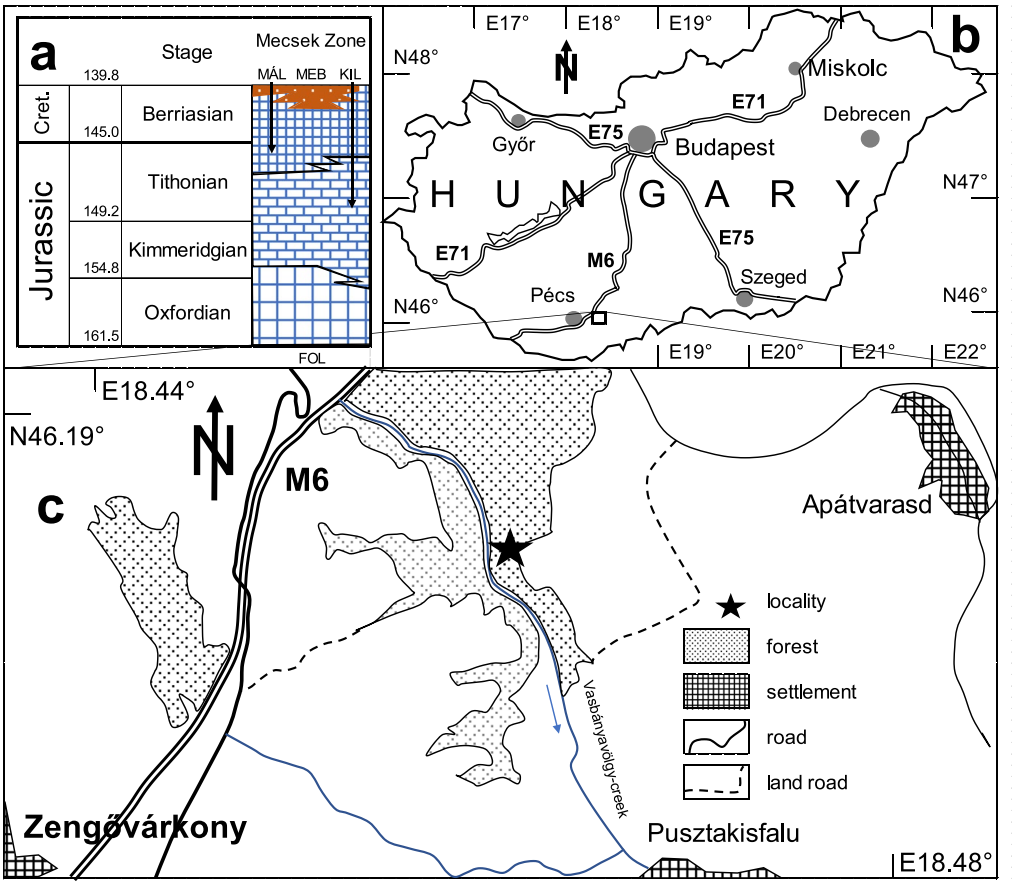
a
Stage
Mecsek Zone
MÁL MEB KIL
139.8
Cret.
145.0
Berriasian
Jurassic
149.2
Tithonian
154.8
Kimmeridgian
161.5
Oxfordian
FOL
b
E17°
E18°
E19°
N48°
Miskolc
E71
Debrecen
Győr
E75
Budapest
H U N G A R Y
N47°
E71
M6
E75
Szeged
Pécs
N46°
N46°
E19°
E20°
E21°
E22°
c
E18.44°
N46.19°
M6
Apátvarasd
locality
forest
settlement
road
land road
Vasbányavölgy-creek
Zengővárkony
Pusztakisfalu
E18.48°

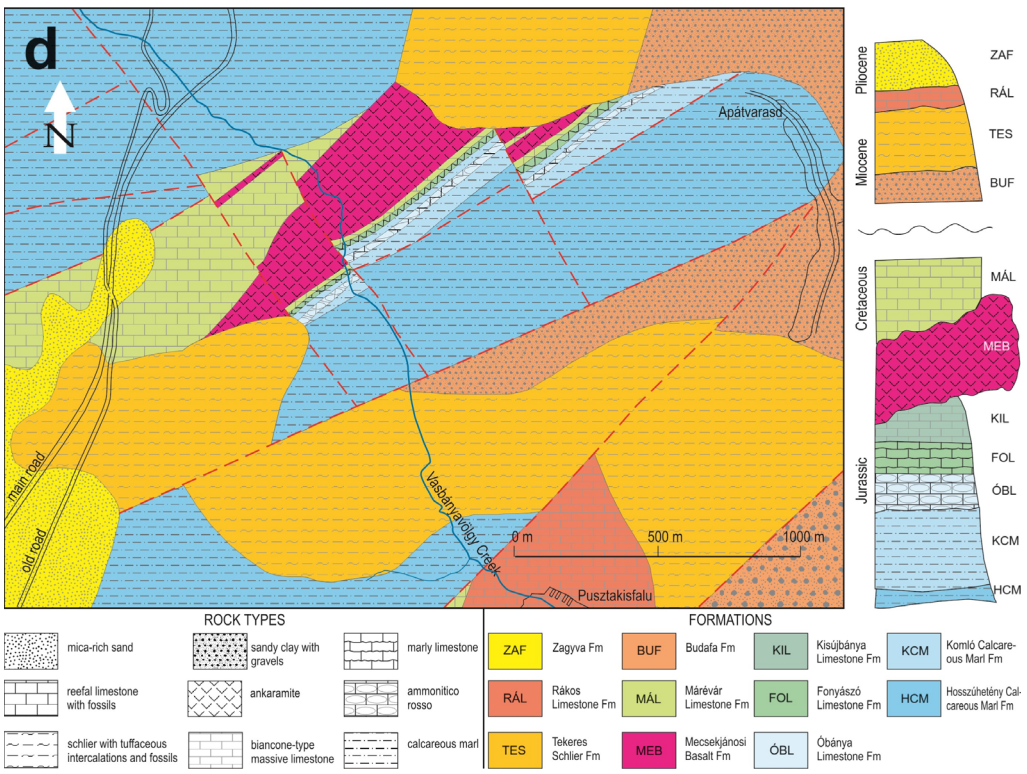
d
N
Apátvarasd
main road
old road
Vasbányavölgy Creek
0 m
500 m
1000 m
Pusztakisfalu
Pliocene
Miocene
ZAF
RÁL
TES
BUF
Cretaceous
Jurassic
MÁL
MEB
KIL
FOL
ÓBL
KCM
HCM
ROCK TYPES
mica-rich sand
sandy clay with gravels
marly limestone
reefal limestone with fossils
ankaramite
ammonitico rosso
schlier with tuffaceous intercalations and fossils
biancone-type massive limestone
calcareous marl
FORMATIONS
ZAF Zagyva Fm
BUF Budafa Fm
KIL Kisújbánya Limestone Fm
KCM Komló Calcareous Marl Fm
RÁL Rákos Limestone Fm
MÁL Márévár Limestone Fm
FOL Fonyászó Limestone Fm
HCM Hosszúhetény Calcareous Marl Fm
TES Tekeres Schlier Fm
MEB Mecsekjánosi Basalt Fm
ÓBL Óbánya Limestone Fm

◂**Fig. 1** Locality map modified from Bujtor and Albrecht (2021) and geological map simplified after Hetényi (et al. 1966). **a** Lithostratigraphic units of the Mecsek Mountains in the Upper Jurassic and Lower Cretaceous from Raucsik (in Főzy 2012). FOL: Fonyászó Limestone Fm; KIL: Kisújbánya Limestone Fm; MEB: Mecsekjánosi Basalt Fm; MÁL: Márévár Limestone Fm. **b** Map of Hungary, with the study area indicated by a rectangle. **c** Simplified map of the study area. **d** Geological map of the study area after Hetényi et al. (1966), simplified. Numeric ages from Cohen et al. (2013)

typical Saccocoma microfacies; and thin, bedded layers with limited thickness. As the Upper Kimmeridgian lithology changes, ammonitico rosso facies disappear and *Cadosina* species appear in microfacies (Nagy 1964). The late Tithonian Age is represented by Maiolica-type sediments and rich calpionellid microfauna.

Maiolica-type sedimentation continued into the Berriasian Age. The sedimentary cycle was terminated by intensified intraplate rifting that brought volcanic material and ended carbonate sedimentation by the Valanginian Age. The age of the sequence is based on the rich but poorly preserved ammonite fauna. Bujtor and Albrecht (2021) state that the ammonite fauna likely represents the Upper Oxfordian Age (mostly the Hypselum Zone) and the lowermost Kimmeridgian (Bimammatum Zone) Age of the sub-Mediterranean-Mediterranean zonal schemes based on the recovered *Trimarginites* cf. *trimarginatus* and *Euaspidoceras* cf. *radisense*. Palaeogeographically the area was still situated close to the source origin, in the vicinity of the southern European shelf (Yilmaz et al. 1996; Dercourt et al. 2000).

Aptychi were first mentioned from the Jurassic of the Mecsek Mountains from Zengővárkony by Böckh (1880). Vadász (1935) mentioned *Laevaptychus latus* (Parkinson, 1811) from the Kimmeridgian at the abandoned quarry in Zengővárkony, close to the locality studied in this paper. It is noteworthy that among the Jurassic Ammonitina families, the morphologies of aptychus differ from each other (Lehmann 1976) and are related to their habitats, functions, and roles (Trauth 1927; Parent et al. 2014). Until this study, there were no attempts to analyse the stable isotope data of Jurassic aptychi from the Mecsek Mountains, Hungary.

Studied sections

The studied section (Fig. 2) is a natural outcrop discovered in a secluded erosional gully by the senior author (LB) and his BSc students in July 2020. The outcrop, which is not indicated on geological maps (Hetényi et al. 1968), is situated in the Eastern Mecsek Mountains, 4 km from Pécsvárad in a NE direction, close to the edge of the Zengővárkony forest, 200 m NE from the lime kilns in the shallow valley of the Vasbányavölgy Creek.

The section is 1 m thick and 5 m in length along strike. The strike and average dip are 305°/40°. The lower part is 46 cm thick and composed of a thick, unstratified, massive, white limestone bank, with occasional red mottling. On average, there are three ammonite specimens per square meter on average on the upper weathered surface of the limestone bank. A nodular, unstratified marly red limestone with very rich but poorly preserved ammonite content (ca. 200 fossil specimens were collected during fieldwork) settled on top of the limestone. This bed is 40 cm thick. The megafauna of the limestone includes annelids, ammonites, aptychi, belemnites, brachiopods, and rarely bivalves and crinoids.

Thin sections revealed wackestone–packstone microfacies with prevailing *Saccocoma* fragments. Besides these planktic elements, a *Globuligerina* sp. foraminifera test fragment was recorded (Bujtor and Albrecht 2021, pl. 1, Fig. 3). Benthic faunal elements are also present: benthic foraminifera *Lenticulina* and *Spirillina* often present, as well as echinoderm test particles, and unidentifiable mollusk or ostracod shell remains are there indicating the presence of a diverse bottom fauna. These results are in line with the macrofaunal composition, which shows the presence of bivalves, echinoderms, and brachiopods with prevailing ammonites (89.2% of the collected specimens, see Bujtor and Albrecht 2021, p. 66, Table 1). The presumed upper and lower continuation of this sequence is obscured by soil and debris.

Results

Textural characteristics of aptychi and brachiopods

The optical microscopic pictures of the 10 aptychi analysed in this study are shown in Fig. 3. The aptychi are composed of two layers, a lower, tubular one and an upper, lamellar layer (cf. Farinacci et al. 1976). The tubular layer is strongly altered, and the chambers are filled with secondary carbonate and silica. The lamellar layer is frequently eroded or dissolved and shows irregular, "cerebral convolution-like" patches of diagenetic carbonate and silica (best shown by specimen OxAM-1023 in Fig. 3). Growth lines are not visible on the outer surface. Eight specimens were drilled from the outside, yielding 4 sub-samples per aptychus, while two specimens (OxAM-1064 and OxAM-1066) were drilled at high resolution, where diagenetic alteration appeared to be less significant, and lamination was preserved. The optical microscopic picture of specimen OxAM-1066 shows the position of the trench.

Sample OxAM-1064 was also investigated by cathodoluminescence microscopy (Fig. 4). Cathodoluminescence microscopy is a powerful tool to detect the diagenetic influences that induce secondary carbonate precipitation or alteration of primary carbonate components. Primary calcite or

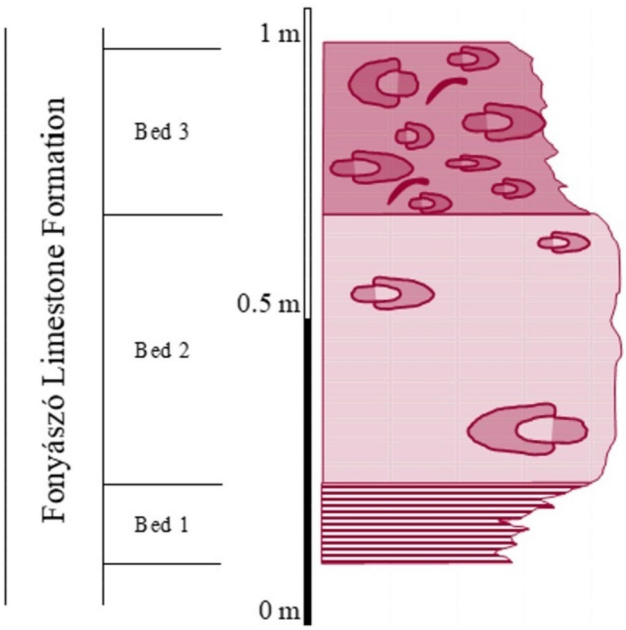

Fig. 2 The studied uppermost Oxfordian–lowermost Kimmeridgian section at Zengővárkony (Mecsek Mountains, Hungary), modified from Bujtor and Albrecht (2021, Fig. 4). Bed 3 yielded the *Laevaptychus* assemblage

aragonite shell materials (e.g., belemnites, ammonites, brachiopods, or mussels) are usually non-luminescent, whereas secondary calcites show orange or red luminescence (e.g., Lukeneder et al. 2010; Colombié et al. 2018; Zuo et al. 2019). Luminescence is a result of the complex interplay of activator (mainly Mn) and quencher (mainly Fe) elements (Hiatt and Pufahl 2014).

Although the chemical composition of carbonate components may indicate a diagenetic influence (Zuo et al. 2019), cathodoluminescence images can be used to select pristine, unaltered shell material on the basis of their non-luminescent character (Colombié et al. 2018). The host rock's carbonate and the calcite cement filling the tubular layer's chambers are strongly luminescent, indicating diagenetic calcite precipitation. Diagenetic calcite also infiltrated the lamellar layer of the aptychi, but the well-preserved part of the lamellar layer is dull. Fe and Mn contents were below detection limits (~0.2 wt%) in all carbonate components (lamellar and tubular layers, host limestone) using EDS-SEM analyses. The yellow rectangles in Fig. 4 indicate the approximate position of the high-resolution drilling trench, situated in a non-luminescent part of the lamellar layer.

Chips were broken from the sampled area of the lamellar layer of the OxAM-1064 aptychus specimen. Scanning electron microscopic (SEM) analyses show a well-preserved crystal structure (Fig. 5a), suggesting that the stable isotope compositions in this section may represent primary signals. The SEM images of sampled brachiopod shell pieces (Fig. 5) show textures of two major layers, in accordance with the shell structure described by Garbelli et al. (2012) for Permian brachiopods and by Roda et al. (2022) for modern brachiopods. The shell of the *Pygope* is well preserved, the texture is dense, and the boundary between the microcrystalline „primary" layer and the columnar "secondary" layer is barely visible (Fig. 5b, c). In contrast, the columnar "secondary " layer of the *Nucleata* shows a granular, altered internal texture on the broken surfaces (Fig. 5d, e), whereas the "primary" layer has secondary carbonate films on the broken surfaces (Fig. 5d, f). Optical microscopic analysis revealed three layers, with one layer almost completely eroded (Fig. 6). The optical microscopic photo of *Pygope catulloi* (Fig. 6a) shows that the internal layer is well preserved. These observations will be compared with stable isotope data in the following subsections.

Stable isotope compositions

The stable isotope compositions obtained in this study are listed in Supplementary Table 1 and shown in Fig. 7, along with the microscope pictures of the samples. The $\delta^{13}C$ values of aptychi sampled at low resolution (Fig. 7a) range from –0.1 to 1.8‰, whereas the $\delta^{18}O$ values scatter in a larger range (from –3.9 to –0.3‰). Within this range, the isotope compositions have no relationship with textural characteristics (e.g., lamellar, or tubular layer). On the other hand, the two specimens (OxAM-1064 and OxAM-1066) investigated at high-resolution display systematic variations. The innermost part of specimen OxAM-1064 sampled the tubular layer and the closest part of the lamellar layer and shows a strong negative $\delta^{18}O$ shift starting from the isotope compositions of the laminated part (Fig. 7a). The $\delta^{13}C$ and $\delta^{18}O$ values of the laminated part scatter in narrow ranges from 0.8 to 2.0‰ and from –1.0 to 0.2‰, respectively, including the outer rim, which shows diagenetic alteration. The least altered part has $\delta^{13}C$ and $\delta^{18}O$ values with narrow ranges ($\delta^{13}C = 0.8$ to 1.7‰, $\delta^{18}O = -0.8$ to –0.2‰). Interestingly, although the outer rim shows signs of diagenetic alteration, the $\delta^{13}C$ and $\delta^{18}O$ values define a positive trend that fits the compositions of the least altered part. Thus, these compositions can be regarded as primary, and the visible diagenetic alteration produced only secondary silica precipitation. The tubular layer of specimen OxAM-1064 was also serially sampled. Its $\delta^{13}C$ values are slightly higher than those of the other samples, and the $\delta^{18}O$ values show a trend from the laminated samples toward negative $\delta^{18}O$ values.

The specimen OxAM-1066 showed a slight $\delta^{18}O$ difference between the samples from the entire laminated layer and the least altered part, depending on the alteration degree, whereas the $\delta^{13}C$ values overlap (Fig. 7b). The least altered laminae have $\delta^{13}C$ and $\delta^{18}O$ values that plot within the least altered field of sample OxAM-1064. The

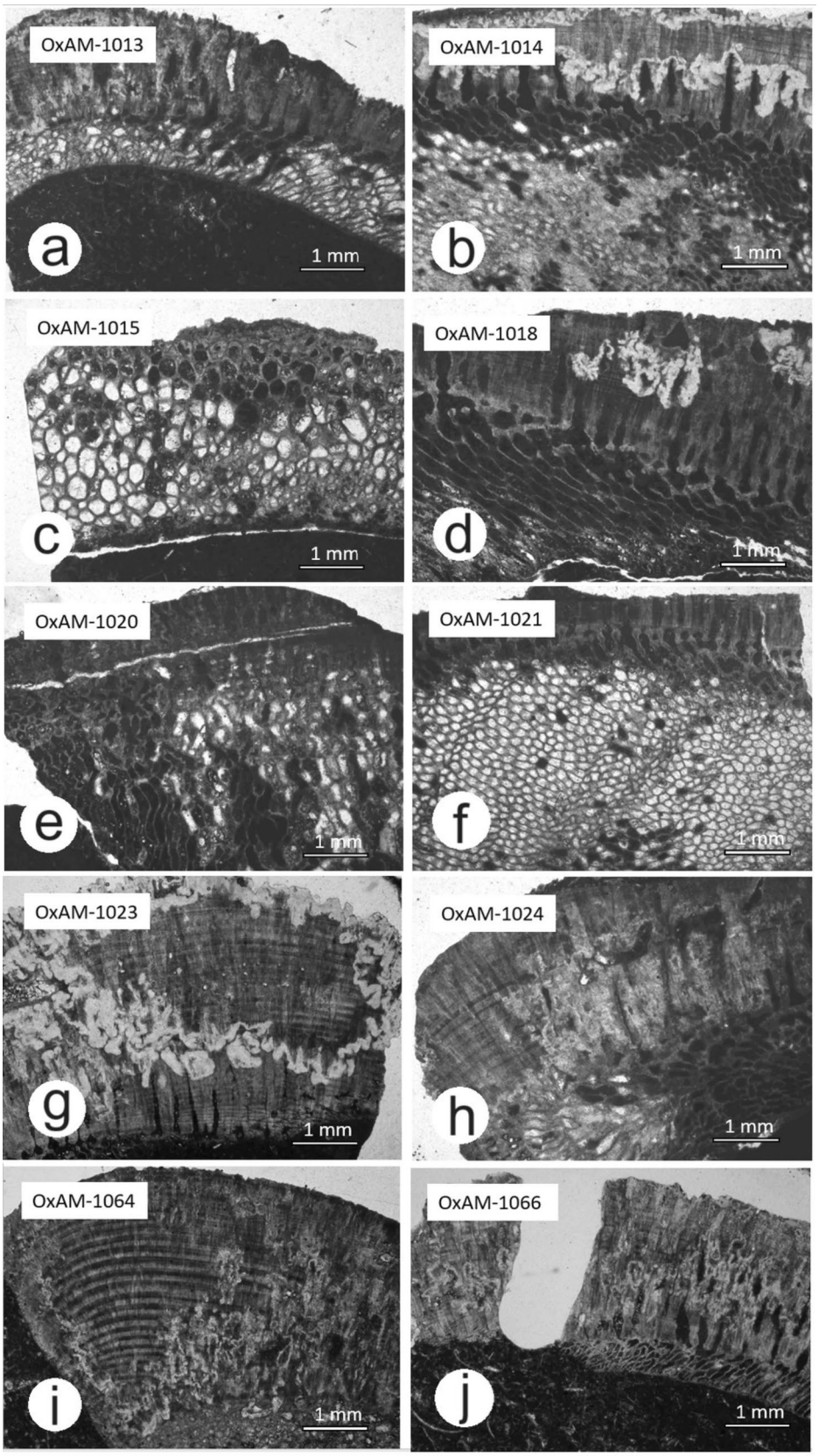

Fig. 3 Optical microscopic images (one Nicol) of the studied aptychi (**a**–**j**). **a**–**f** Processed samples did not preserve the lamellar structure but only the tubular parts. **g**–**i** Processed samples reveal the lamellar structures with variously preserved concentric structures. **j** Sampling track in the tubular layer. Abbreviations correspond to the following repository numbers: OxAM-1013: J 2020.691.1; OxAM-1014: J 2020.692.1; OxAM-1015: J 2020.693.1; OxAM-1018: J 2020.696.1; OxAM-1020: J 2020.698.1; OxAM-1021: J 2020.699.1; OxAM-1023: J 2020.701.1; OxAM-1024: J 2020.702.1; OxAM-1064: J 2020.743.1; OxAM-1066: J 2020.745.1. Scale bars indicate 1 mm

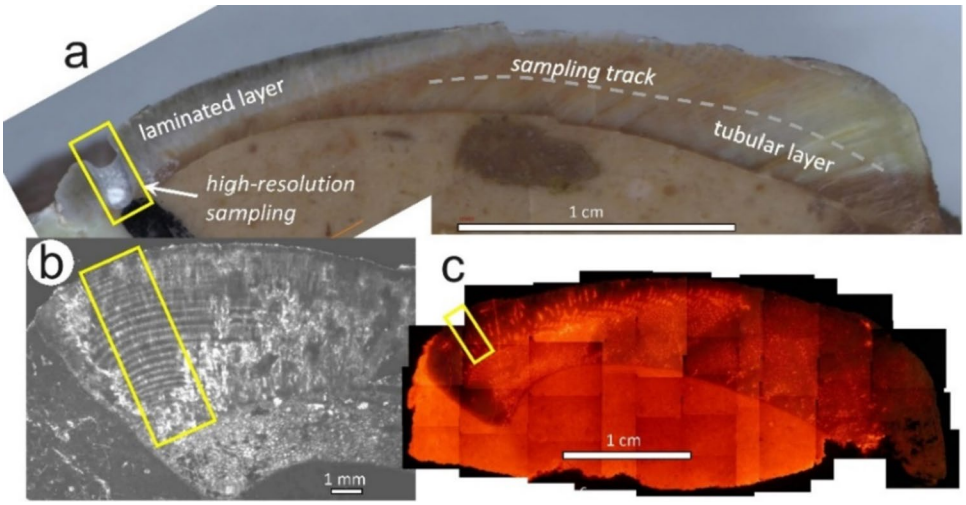

Fig. 4 **a** Binocular, **b** optical (crossed nicols), and **c** cathodoluminescence microscopic pictures of OxAM-1064. The yellow rectangles indicate the site of trench drilling

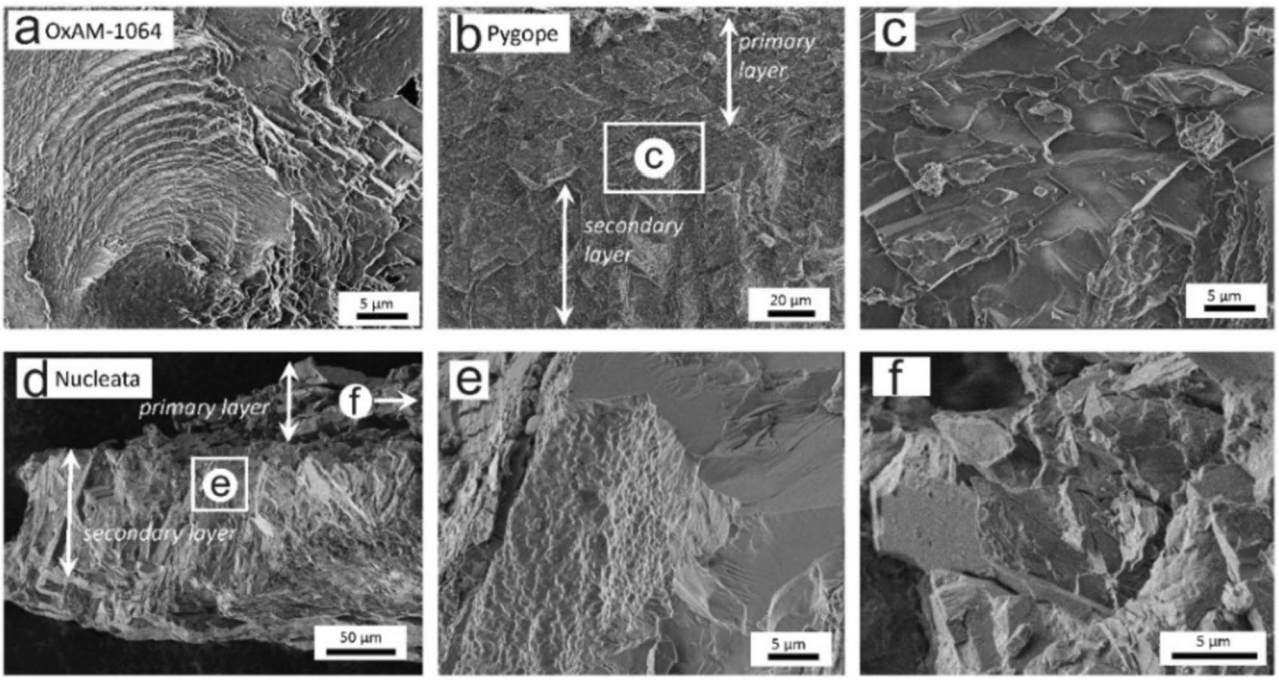

Fig. 5 Scanning electron microscopic images of **a** *Laevaptychus* OxAM-1064, **b**, **c** *Pygope catulloi* J 2020.593.1 sample, and **d**, **e**, **f** *Nucleata bouei* J 2020.592.1 shell samples

carbon and oxygen isotope compositions of brachiopod shells fit into the ranges of aptychi (Fig. 7b). Both brachiopods were sampled at two points, where the best-preserved shell pieces could be collected under the binocular microscope. The $\delta^{18}O$ values (–2.7 and –1.1‰) of brachiopod *Nucleata bouei* are significantly more negative than those of *Pygope catulloi* ($\delta^{18}O = -0.8$ and –0.4‰). The $\delta^{13}C$ values (–1.8‰ for the *Nucleata bouei* and –2.0 and –1.7‰ for the *Pygope catulloi*) are practically the same for both brachiopods and fit in with the field of aptychi (Fig. 7b).

Discussion

Preservation vs. diagenesis

Primary compositions that are free of diagenetic effects should be selected when estimating paleoenvironmental conditions. This is possible using textural characteristics (e.g., Kruta et al. 2014) or by evaluating stable isotope trends. Diagenesis of carbonate sediments has been

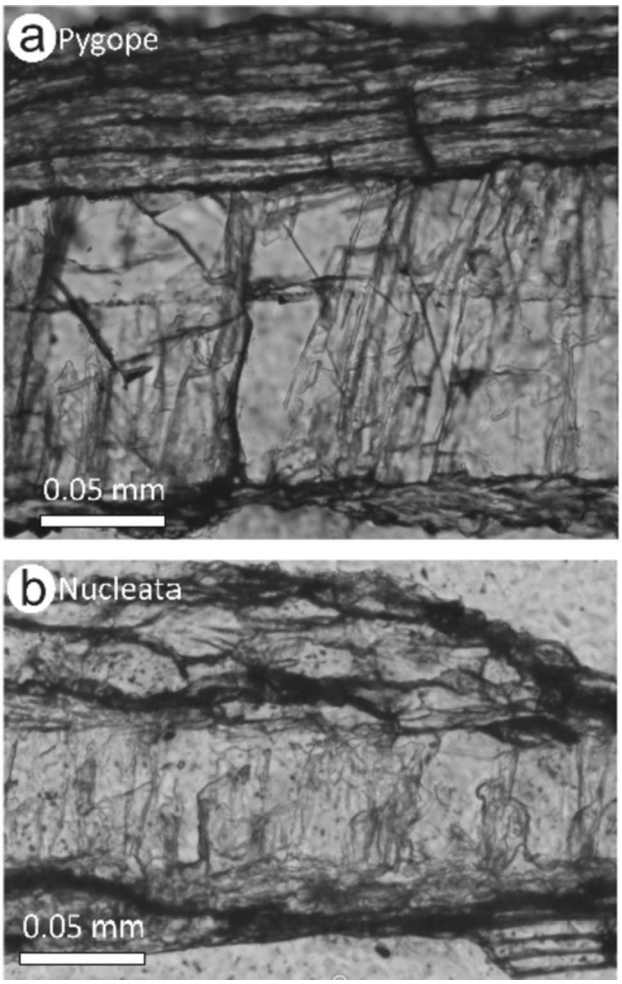

Fig. 6 Optical microscopic photos of brachiopod shells. Sections are perpendicular to shell surfaces (with one nicol). **a** *Pygope catulloi*, sample J 2020.593.1; **b** *Nucleata bouei*, sample J 2020.592.1

extensively studied, with thousands of articles discussing stable isotope compositions that reflect diagenetic effects. As such, the reader is referred to one of the handbooks that reviews diagenetic influences (e.g., Hoefs 2009). Diagenesis of carbonate rocks may result in the precipitation of secondary carbonate in voids or in the dissolution and reprecipitation of unstable carbonate (e.g., aragonite in the ammonite shells). Stable oxygen isotope compositions of carbonate are determined by the $\delta^{18}O$ value of the solution and the formation temperature (McCrea 1950). A temperature increase during diagenesis would result in a decrease in oxygen isotope fractionation between the marine carbonate material and the pore fluids, shifting the $\delta^{18}O$ value toward the water's composition, i.e., in a negative direction. In the case of meteoric water infiltration, the interaction with relatively ^{18}O-depleted meteoric water again results in low $\delta^{18}O$ values. A positive shift in the carbonate $\delta^{18}O$ values might appear if ^{18}O-enriched solutions react with the carbonate rock, or if the formation temperature of secondary, diagenetic carbonate is significantly lower than the marine carbonate's deposition temperature. These cases are very rare, so it can be stated that diagenesis is generally reflected by lowered $\delta^{18}O$ values (e.g., Hoefs 2009). Stable carbon isotope compositions are around 0‰ (relative to V-PDB) for marine carbonate formations. Burial diagenesis may mobilize oxidized organic carbon with low ^{13}C contents, i.e., low $\delta^{13}C$ values. Infiltration of meteoric water containing soil-derived carbon may also carry a low $\delta^{13}C$ signal. To summarize, if oxidized organic carbon is mobilized and involved in the formation of diagenetic carbonate, the $\delta^{13}C$ value of the bulk carbonate is shifted in a negative direction, along with lower $\delta^{18}O$ values, whereas if diagenesis was not associated with mobilization or organic carbon, it is reflected only by low $\delta^{18}O$ values (Hoefs 2009).

The aptychi studied at low resolution show a negative $\delta^{18}O$ shift from the $\delta^{13}C$–$\delta^{18}O$ field of the least altered laminae of OxAM-1064 and OxAM-1066, which may indicate diagenesis. The $\delta^{18}O$ values (with an assumed global mean seawater $\delta^{18}O_{sw}$ value of –1‰, Shackleton and Kenneth 1975) would correspond to temperatures reaching 30 °C if the equation of Anderson and Arthur (1983) is used (Fig. 7a). On the other hand, the OxAM-1064 and OxAM-1066 aptychi showed thin (approximately 0.1 mm) lamination (Fig. 3) with a well-preserved internal crystal structure (Fig. 5a), suggesting preservation of primary textures and compositions. The well-preserved tubular layer of OxAM-1064 has diagenetic oxygen isotope compositions, indicating that the $\delta^{18}O$ values of calcites collected from the aptychus surface (e.g., Machalski et al. 2021) must be interpreted with caution.

The microscopic observations presented in this study may also provide information on the lamellar layer of Aspidoceratidae. The lamellar layer of OxAM-1064 contains about 24 laminae, although it should be noted that the innermost part of the layer is altered, so some laminae may be missed. Another sample, OxAM-1023 (see Fig. 3), contains 32 laminae, with the very thin ones in the innermost part. Although the exact meaning of lamination is not clear at present, it can be concluded that the laminae are primary features, whose appearance without secondary mineral precipitation can indicate preservation of primary isotope compositions.

Another approach for proving the non-diagenetic nature of stable isotope compositions is to analyse different carbonate-secreting organisms. The shell of *Pygope catulloi* examined in this study showed much fewer signs of alteration by SEM analyses than the shell of *Nucleata bouei*. Its $\delta^{18}O$ value (-0.6 ± 0.2‰) is close to the least altered lamina values (Fig. 7), supporting the unaltered state of the sample. The two pieces of the *Nucleata bouei* shell yielded identical $\delta^{13}C$ (both 1.8‰) but very different $\delta^{18}O$ values (–2.7 and

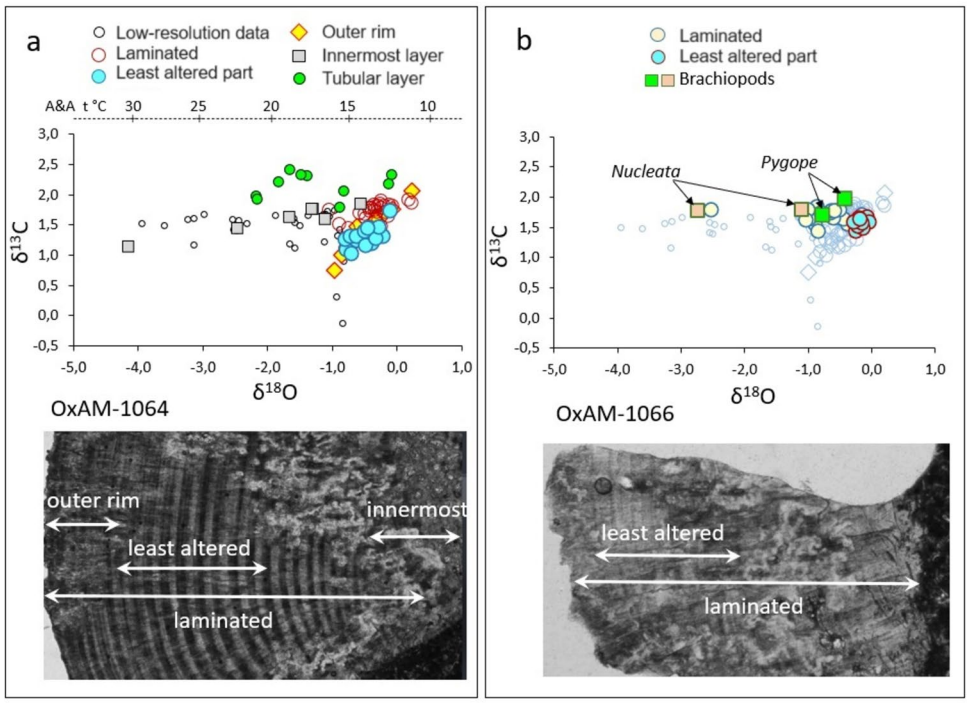

Fig. 7 Stable carbon and oxygen isotope compositions (in ‰ relative to V-PDB) of the OxAM-1064 (**a**), and OxAM-1066 (**b**) aptychi, as well as the *Pygope catulloi* (specimen J 2020.593.1) and *Nucleata bouei* (specimen J 2020.592.1) brachiopod shells. Paleotemperatures were calculated using the equation of Anderson and Arthur (1983) and a $\delta^{18}O_{sw}$ value of –1‰ (Shackleton and Kenneth, 1975). The low-resolution data obtained for aptychi are shown in Fig. 3. The sampling track in the tubular layer of sample OxAM-1064 is shown in Fig. 4a. The microscopic images and sampled parts whose data are separately plotted are shown in the lower panels in **a** and **b**

–1.1‰). The large $\delta^{18}O$ variation and the negative shift are in accordance with the altered state of the shell.

Thus far, only a few stable isotope studies have been conducted on aptychi, and these are not associated with careful petrographic analyses so as not to damage the specimens. Comparing the $\delta^{13}C$ and $\delta^{18}O$ values of aptychi analysed by Price and Sellwood (1994) (Fig. 8), their samples were likely diagenetically affected. It should be noted that they sampled the tubular layer ("honeycomb structure"), which may contain diagenetic calcite cement, as shown here. Although Kruta et al. (2014) conducted a careful textural analysis using SEM, even the samples with high degree of

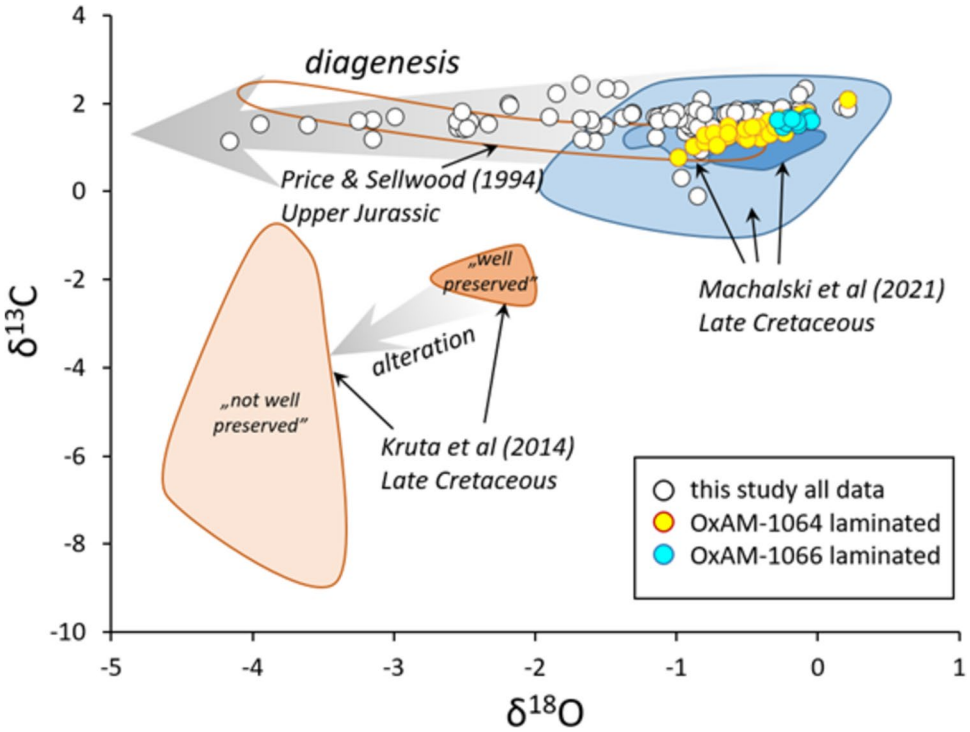

Fig. 8 Stable carbon and oxygen isotope compositions (in ‰ relative to V-PDB) of the aptychi studied in this paper, as well as published data on aptychus calcite

preservation had low $\delta^{18}O$ values (Fig. 8), which would correspond to elevated ambient temperatures or to an influx of low $\delta^{18}O$ water into the sea. They may also indicate cryptic diagenesis that was not revealed by the textural observations. Machalski et al. (2021) used a combination of cathodoluminescence (CL) microscopic and SEM observations to select unaltered samples, and on the basis of the $\delta^{18}O$ fluctuations in serial sub-samples, they excluded significant diagenetic effects. Although their $\delta^{13}C$ and $\delta^{18}O$ ranges are similar to compositions in this study (Fig. 8), their scatter is much larger. These observations indicate that SEM analysis may only detect strong diagenesis, while the effects of small amounts of secondary calcite or late-stage isotope exchange would not be revealed. However, the optical microscopic analysis, combined with CL and SEM measurements, as presented in this study, can be effectively used to select primary compositions.

Paleotemperatures during the late Jurassic

Oxygen isotope thermometry is based on the temperature-dependent fractionation of the ^{18}O and ^{16}O isotopes between oxygen-bearing compounds, which in our case is between calcite and seawater. The fractionation is expressed as $1000 \cdot \ln\alpha$ value, where $\alpha = (^{18}O/^{16}O_{calcite})/(^{18}O/^{16}O_{water})$. Although the thermometric equation for aptychus calcite cannot be calibrated with modern data, as ammonites are extinct, the equation used for belemnites, another Mesozoic calcite-secreting cephalopod, can be applied. As Vickers et al. (2020) determined based on clumped isotope measurements, the equation of Daëron et al. (2019) can be used for belemnites, so the same equation will be used in this paper for aptychus calcite:

$$1000 \cdot \ln\alpha = 17570/T - 29.13,$$

where T is temperature in kelvin. In contrast to the belemnites, the fractionation equation for brachiopods can be calibrated with modern, living specimens. Brand et al. (2019) provided the equation:

$$T\,(^{\circ}C) = 17.3750 - 4.2535 \cdot (\delta_c - \delta_{sw}) + 0.1473 \cdot (\delta_c - \delta_{sw})2,$$

where δ_c is the $\delta^{18}O$ value of calcite relative to V-PDB, and δ_{sw} is the $\delta^{18}O$ value of seawater relative to V-SMOW (Vienna Standard Mean Ocean Water).

Aspidoceratid ammonites, the host of laevaptychi, lived in a water column of at least 100 m deep, far from coastal regions (Gygi 2003). Our study area (the Mecsek Mountains, Tisza microcontinent) was within the Tethys Ocean realm, close to the northern shelf (Yilmaz et al. 1996; Dercourt et al. 2000). As a result, local influences, like freshwater influx or evaporation in a closed basin, can be excluded, and the global relationship of latitudinal $\delta^{18}O_{sw}$ variations can be applied following the procedure of Alberti et al. (2020). The paleogeographic position of the Mecsek Mountains has been estimated around 30–35°N by Yilmaz et al. (1996) and Márton (2000), about 25°N by Dercourt et al. (2000), and about 40°N by Hinsbergen et al. (2020), thus, a position of 30 ± 5°N is assumed. This latitude would correspond to a $\delta^{18}O_{sw}$ value of –0.2‰ following Alberti et al. (2020).

The $\delta^{18}O$ values of the laminated calcite of the OxAM-1064 and OxAM-1066 aptychi cover the range of –1.0 to 0.2‰, which corresponds to a temperature range of 20 to 26 °C using the equation of Daëron et al. (2019) and the $\delta^{18}O_{sw}$ value of –0.2‰. As diagenesis would shift the $\delta^{18}O$ value of the aptychus calcite in a negative direction, the highest $\delta^{18}O$ value of the laminated calcite corresponds to a primary composition, as well as to the lowest temperature that the animal experienced, i.e., 20 °C. The lowest unaltered oxygen isotope composition would be –1.0 ‰, which corresponds to 26 °C. Thus, we can assume that the aspidoceratid ammonite containing the studied *Laevaptychus* either migrated into the water column with a temperature range of 20 to 26 °C, or the water temperature and/or water $\delta^{18}O$ value fluctuated during the precipitation of the aptychus calcite. The latter value is closest to the sea surface temperature (SST) data of Lukeneder (2015), although the ammonites lived deeper in the water column. Lukeneder (2015) compared recently living cephalopods and Mesozoic (middle Jurassic and Cretaceous) ammonites and obtained seawater temperatures from 12 °C up to 29 °C, depending on the ammonite taxa, as well as its ontogenetic evolution and migrations. Jenkyns et al. (2012) reported even higher SSTs (26 to 30 °C) using TEX_{86} analyses of middle Jurassic to lower Cretaceous sediments from the southern Atlantic Ocean.

The studied brachiopods (*Pygope catulloi* and *Nucleata bouei*) lived on the seafloor, i.e., at a lower temperature than the ammonites did. The highest (least altered) $\delta^{18}O$ value of *P. catulloi* is –0.4 ‰, which corresponds to 18.2 °C using the $\delta^{18}O_{sw}$ value of –0.2 ‰ and the equation of Brand et al. (2019). This is slightly lower than the lower limit of the aptychus-based temperature, in accordance with the difference in habitat (water column vs. seafloor water), although we must note that diagenesis may have affected even the shell of *Pygope catulloi,* making the temperature of 18 °C an upper limit.

These seawater temperature values can be compared with global data (Valdes et al. 2021), taking latitudinal temperature and seawater composition changes into account (Shea et al. 1992; Alberti et al. 2020; Sadji et al. 2021; Alberti et al. 2022a, b). Alberti et al. (2022a) presented a global compilation of SST data based on belemnite, mollusc, and brachiopod $\delta^{18}O$ analyses, as well as latitudinal variations of paleotemperatures during the Callovian. The Callovian latitude–temperature relationships follow the recent one (Shea et al. 1992), but with

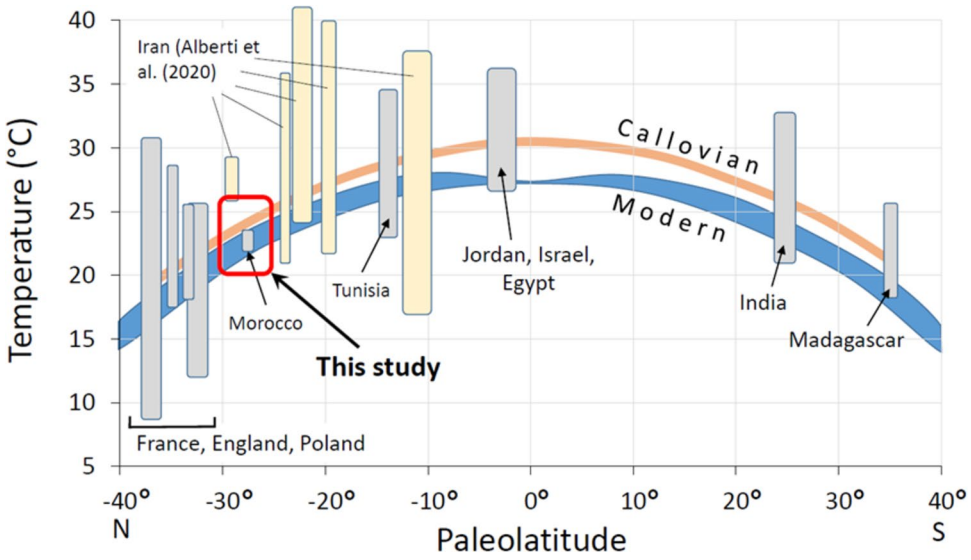

Fig. 9 Latitudinal changes of Jurassic paleotemperatures (modified from Alberti et al. 2022a) and the temperature range obtained in this study

temperatures that are 2–3 °C higher (Fig. 9). The Jurassic shell and belemnite data compiled by Alberti et al. (2022a) generally fit the Callovian curve, but the scatter reaches 10–20 °C. Although the global climate conditions may have been different in the Callovian than in the Oxfordian-Kimmeridgian (Dera et al. 2011), the Callovian latitude–temperature relationship presented by Alberti et al. (2022a) may serve as a reference for the present data, as well, especially considering the large scatter in paleotemperature data. The aptychus-based seawater temperature range of 23 ± 3 °C is in good agreement with the Jurassic data shown in Fig. 9, as well as with the Jurassic and Cretaceous marine latitude–temperature relationships (based on belemnite-bivalve-TEX_{86} temperatures and climate simulations) that were compiled by Letulle et al. (2022). These agreements and the small scatter of the reconstructed temperature range indicate that aptychus calcite potentially offers a good paleotemperature archive, provided that diagenetic effects can be excluded or filtered out using careful microtextural and petrographic analyses. Excellent Jurassic control samples may be collected from the pelagic zone, where aptychi are usually collected. Aptychi and sessile discolioide brachiopods are usually preserved together, yielding good control samples in situ with which to verify the palaeotemperature data acquired from aptychi. However, the use of laevaptychi is time-restricted from the middle Callovian to the Berriasan Ages, when aspidoceratid ammonites lived (Engeser and Keupp 2002).

Conclusions

Well-preserved late Oxfordian to early Kimmeridgian laevaptychi were examined using optical and cathodoluminescence microscopy, scanning electron microscopy (SEM), and stable isotope mass spectrometry to select pristine, unaltered calcite material and to calculate seawater temperatures. Optical and SEM analyses revealed a well-expressed lamination in the upper lamellar layer of *Laevaptychus* that may indicate preservation of original structures and compositions. The combined evaluation of microscopic observations and stable carbon and oxygen isotope compositions allowed for the detection of diagenetic effects that modified the original isotopic compositions. Pristine, unaltered compositions were used to calculate seawater temperatures, yielding a range of 20 to 26 °C, which is in good agreement with published Jurassic seawater temperatures. Rare brachiopod samples were also investigated, and the least altered samples were selected for SEM analysis. The stable oxygen isotope composition of *Pygope catulloi* corresponds to a seawater temperature of 18 °C, which is slightly lower than the 20 to 26 °C range obtained from the aptychi and is consistent with the benthic character of *Pygope*. This study shows that the well-preserved calcite material of aptychi represents a valuable paleotemperature archive.

Supplementary Information The online version contains supplementary material available at https://doi.org/10.1007/s00531-023-02376-5.

Acknowledgements The authors are grateful to the BSc students of Pécs University (Ákos Miklósy and Richárd Albrecht) for cleaning the outcrop section during fieldwork in 2020 and 2021. Dr. Ariana Gugora kindly improved the English of the manuscript, which is gratefully acknowledged. The authors highly appreciate the supportive and constructive comments of the Editor-in-Chief Ulrich Riller, Topic Editor Sascha Flögel, and the two anonymous reviewers that greatly improved the quality of this paper.

Author contributions Fieldwork was done by LB. The research idea was proposed by LB. The research concept and design were proposed by AD. Material preparation, data collection, and analysis were conducted by AD. Instrumental measures, analyses, and interpretation

were completed by PN and BB. The manuscript was written by the authors, and all authors read and approved the final manuscript.

Funding Open access funding provided by Eszterhazy Karoly Catholic University.

Declarations

Conflict of interest The authors declare that they have no known competing financial interests or personal relationships that may have influenced the work detailed herein.

References

Alberti M, Leshno Y, Fürsich FT, Edelman-Furstenberg Y, Andersen N, Garbe-Schönberg D (2020) Stress in the tropics? Impact of a latitudinal seawater $\delta^{18}O$ gradient on Middle Jurassic temperature reconstructions at low latitudes. Geology 48:1210–1215. https://doi.org/10.1130/G47824.1

Alberti M, Fürsich FT, Andersen N (2022a) First estimates for Jurassic seawater temperatures based on oxygen isotope analyses of calcitic fossils from Central Iran: evidence for a major plate tectonic shift? J Asian Earth Sci 236:105338. https://doi.org/10.1016/j.jseaes.2022.105338

Alberti M, Fürsich FT, Pandey DK, Mukherjee D, Andersen N, Garbe-Schönberg D (2022b) Middle to Late Jurassic stable isotopes and element ratios of fossils from western India: developing a reference temperature curve for northeastern Gondwana. Global Planet Change 212:103795. https://doi.org/10.1016/j.gloplacha.2022.103795

Anderson TF, Arthur MA (1983) Stable isotopes of oxygen and carbon and their application to sedimentological and paleoenvironmental problems. In: Arthur MA, Anderson TF, Kaplan IR, Veizer J, Land L (eds) Stable isotopes in sedimentary geology, vol 10. SEPM Short Course, pp 1–151

Böckh J (1880) Adatok a Mecsekhegység és dombvidéke jurakorbeli lerakodásainak ismeretéhez. I. Stratigraphiai rész. Értekezések a Természettudományok Köréből 10(10):1–50

Brand U, Bitner MA, Logan A, Azmy K, Crippa G, Angiolini L, Colin P, Griesshaber E, Harper EM, Taddei Ruggiero E, Häussermann V (2019) Brachiopod-based oxygen-isotope thermometer: update and review. Riv It Pal Strat 125:775–787. https://doi.org/10.13130/2039-4942/12226

Bujtor L, Albrecht R (2021) Latest Oxfordian—earliest Kimmeridgian ammonite dominated fauna and microfacies from the ammonitico rosso-type Fonyászó Limestone Formation at Zengővárkony (Mecsek Mountains, Hungary). Volumina Jur 19:61–96. https://doi.org/10.7306/VJ.19.3

Bujtor L, Albrecht R (2022) Oxfordian brachiopods from the ammonitico rosso-type Fonyászó Limestone formation at Zengővárkony, Mecsek Mountains, Hungary and their palaeoecological, palaeobiogeographical and palaeopathological significance. Paläont Zeitschrift 96:51–65. https://doi.org/10.1007/s12542-021-00560-z

Cohen KM, Finney SC, Gibbard PL, Fan J-X (2013) The ICS international chronostratigraphic chart. Episodes 36:199–204. https://doi.org/10.18814/epiiugs/2013/v36i3/002

Colombié C, Carcel D, Lécuyer C, Ruffel A, Schnyder J (2018) Temperature and cyclone frequency in Kimmeridgian Greenhouse period (late Jurassic). Global Planet Change 170:126–145. https://doi.org/10.1016/j.gloplacha.2018.08.005

Csontos L, Vörös A (2004) Mesozoic plate tectonic reconstruction of the Carpathian region. Palaeogeogr Palaeoclimat Palaeoecol 210:1–56. https://doi.org/10.1016/j.palaeo.2004.02.033

Daëron M, Drysdale RN, Peral M, Huyghe D, Blamart D, Coplen TB, Lartaud F, Zanchetta G (2019) Most Earth-surface calcites precipitate out of isotopic equilibrium. Nature Comm 10:429. https://doi.org/10.1038/s41467-019-08336-5

Dera G, Brigaud B, Monna F, Laffont R, Pucéat E, Deconinck J-F, Pellenard P, Joachimski MM, Durlet C (2011) Climatic ups and downs in a disturbed Jurassic world. Geology 39:215–218. https://doi.org/10.1130/G31579.1

Dercourt J, Gaetani M, Vryelinck B, Barrier E, Biju-Duval B, Brunet MF, Cadet JP, Crasquin S, Sandulescu M (2000) Atlas Peri-Tethys, paleogeographical maps. CCGM/CGMW, Paris

Engeser T, Keupp H (2002) Phylogeny of the aptychi-possessing Neoammonoidea (Aptychophora nov., Cephalopoda). Lethaia 34:79–96

Farinacci A, Mariotti N, Matteucci R, Nicosia U, Pallini G (1976) Structural features of some Jurassic and Early Cretaceous Aptychi. Boll Soc Pal Ital 15(2):111–143

Főzy I (2012) Magyarország litosztratigráfiai alapegységei. Jura. Magyar Állami Földtani Intézet, Budapest

Galácz A (1984) Jurassic of Hungary: a review. Acta Geol Hung 27(3–4):359–377

Garbelli C, Angiolini L, Jadoul F, Brand U (2012) Micromorphology and differential preservation of Upper Permian brachiopod low-Mg calcite. Chem Geol 298–299:1–10. https://doi.org/10.1016/j.chemgeo.2011.12.019

Gygi RA (2003) Perisphinctacean ammonites of the Late Jurassic in northern Switzerland: a versatile tool to investigate the sedimentary geology of an epicontinental sea. Mém Suisses Pal 123:1–232

Haas J, Cs P (2004) Mesozoic evolution of the Tisza Megaunit. Int J Earth Sci 93(2):297–313. https://doi.org/10.1007/s00531-004-0384-9

Heténi R, Hámor G, Nagy I (1966) A Mecsek-hegység földtani térképe 10000-es sorozat Apátvarasd. Geological Institute of Hungary, Budapest

Heténi R, Hámor G, Nagy I (1968) Magyarázó a Mecsek Hegység Földtani Térképéhez, 10.000-es sorozat, Apátvarasd. Geological Institute of Hungary, Budapest

Hiatt EE, Pufahl PK (2014) Cathodoluminescence petrography of carbonate rocks: application to understanding diagenesis, reservoir quality, and pore system evolution. In: Coulson I (ed) Cathodoluminescence and its application to geoscience, vol 45. Mineralog Assoc Canada, Short Course Series, pp 75–96

Hoefs J (2009) Stable isotope geochemistry. Springer-Verlag Berlin Heidelberg

Jautzy JJ, Savard MM, Dhillon RS, Bernasconi SM, Smirnoff A (2020) Clumped isotope temperature calibration for calcite: bridging theory and experimentation. Geochem Persp Lett 14:36–41. https://doi.org/10.7185/geochemlet.2021

Jenkyns HC, Schouten-Huibers L, Schouten S, Sinninghe Damsté JS (2012) Warm Middle Jurassic-Early Cretaceous high-latitude sea-surface temperatures from the Southern Ocean. Clim past 8:215–226. https://doi.org/10.5194/cp-8-215-2012

Johnston VE, Borsato A, Spötl C, Frisia S, Miorandi R (2013) Stable isotopes in caves over altitudinal gradients: fractionation behaviour and inferences for speleothem sensitivity to climate change. Clim past 9:99–118. https://doi.org/10.5194/cp-9-99-2013

Kruta I, Landman NH, Cochran JK (2014) A new approach for the determination of ammonite and nautilid habitats. PLoS ONE 9(1):e87479. https://doi.org/10.1371/journal.pone.0087479

Landis GP (1983) Harding Iceland Spar: a new $\delta^{18}O$-$\delta^{13}C$ carbonate standard for hydrothermal minerals. Isotope Geosci 1:91–94. https://doi.org/10.1016/S0009-2541(83)80008-4

Lehmann U (1976) Ammoniten ihr Leben und ihre Umwelt. Enke-Verlag, Stuttgart

Letulle T, Suan G, Daëron M, Rogov M, Lécuyer C, Vinçon-Laugier A, Reynard B, Montagnac G, Lutikov O, Schlögl J (2022) Clumped isotope evidence for Early Jurassic extreme polar warmth and high climate sensitivity. Clim past 18:435–448. https://doi.org/10.5194/cp-18-435-2022

Lukeneder A (2015) Ammonoid habitats and life history. In: Klug C, Korn D, der Baets K, Kruta I, Mapes R (eds) Ammonoid paleobiology: from anatomy to ecology. Topics in geobiology, vol 43. Springer, Dordrecht. https://doi.org/10.1007/978-94-017-9630-9_18

Lukeneder A, Harzhauser M, Müllegger S, Piller WE (2010) Ontogeny and habitat change in Mesozoic cephalopods revealed by stable isotopes ($\delta^{18}O$, $\delta^{13}C$). Earth Planet Sci Lett 296:103–114. https://doi.org/10.1016/j.epsl.2010.04.053

Machalski M, Owocki K, Dubicka Z, Malchyk O, Wierny W (2021) Stable isotopes and predation marks shed new light on ammonoid habitat depth preferences. Sci Rep 11:22730. https://doi.org/10.1038/s41598-021-02236-9

Márton E (2000) The Tisza Megatectonic Unit in the light of paleomagnetic data. Acta Geol Hung 43(3):329–343

McCrea JM (1950) On the isotopic chemistry of carbonates and a paleotemperature scale. J Chem Phys 18(6):849–857. https://doi.org/10.1063/1.1747785

Moore GT, Hayashida DN, Ross CA, Jacobson SR (1993) Late Jurassic paleoclimate of Pangea based on results from a General Circulation Model. In: Oremland RS (ed) Biogeochemistry of global change. Chapman & Hall Inc, pp 61–79

Nagy I (1964) Examen microbiofacial du complexe du Malm en affleurement à Zengővárkony (Montagne Mecsek). A Magyar Állami Földtani Intézet Évi Jelentése az 1961. évről (I.):97–108

O'Neil JR, Clayton RN, Mayeda TK (1969) Oxygen isotope fractionation in divalent metal carbonates. J Chem Phys 51:5547–5558

Parent H, Westermann GEG, Chamberlain JA (2014) Ammonite aptychi: functions and role in propulsion. Geobios 47:45–55. https://doi.org/10.1016/j.geobios.2013.12.001

Price GD, Sellwood BW (1994) Palaeotemperatures indicated by Upper Jurassic (Kimmeridgian-Tithonian) fossils from Mallorca determined by oxygen isotope composition. Palaeogeo Palaeoclimat Palaeoecol 110:1–10

Ruckwied K, Götz AE, Pálfy J, Török Á (2008) Palynology of a terrestrial coal-bearing series across the Triassic/Jurassic boundary (Mecsek Mts, Hungary). Cent Eur Geol 51(1):1–15. https://doi.org/10.1556/ceugeol.51.2008.1.1

Sadji R, Munnecke A, Benhamou M, Alberti M, Belkhedim S, Ramdane N (2021) Late Jurassic temperatures for the southern Tethyan margin based on belemnites $\delta^{18}O$ from the Ouarsenis Mountains, northwestern Algeria. Palaeogeogr Palaeoclimat Palaeoecol 566:110224. https://doi.org/10.1016/j.palaeo.2021.110224

Sellwood BW, Valdes PJ (2006) Mesozoic climates: general circulation models and the rock record. Sediment Geol 190:269–287. https://doi.org/10.1016/j.sedgeo.2006.05.013

Shackleton NJ, Kennett JP (1975) Paleotemperature history of the Cenozoic and the initiation of Antarctic glaciation: oxygen and carbon isotope analyses in DSDP sites 277, 279, and 281. Init Rep Deep Sea Drill Proj 29:743–755

Shea DJ, Trenberth KE, Reynolds RW (1992) A global monthly sea surface temperature climatology. J Climat 5:987–1001

Simonet Roda M, Griesshaber E, Angiolini L, Rollion-Bard C, Harper EM, Bitner MA, Milner Garcia S, Ye F, Henkel D, Häussermann V, Eisenhauer A (2022) The architecture of Recent brachiopod shells: diversity of biocrystal and biopolymer assemblages in rhynchonellide, terebratulide, thecideide and craniide shells. Mar Biol 169:1–52. https://doi.org/10.1007/s00227-021-03962-4

Tari G (2015) The palinspastic position of Tisia (Tisza) in the Alpine realm: a view from the outside of the Pannonian Basin. In: Tisia Conference 27–28 February, 2015, Pécs, Dályay V, Sámson M (ed), Molnár Nyomda és Kiadó, Pécs, Hungary pp 29-32

Trauth EF (1927–1936) Aptychenstudien I–VII: Wien, Annal Naturhist Mus 41:171–259 (1927); 42:171–259 (1928); 44:329–411 (1930); 45: 17–136 (1931); 47:127–145 (1936)

Tremaine DM, Froelich PN, Wang Y (2011) Speleothem calcite farmed in situ: Modern calibration of $\delta^{18}O$ and $\delta^{13}C$ paleoclimate proxies in a continuously-monitored natural cave system. Geochim Cosmochim Acta 75:4929–4950. https://doi.org/10.1016/j.gca.2011.06.005

Vadász E (1935) Das Mecsek-Gebirge. Geologische Beschreibung ungarischer Landscahften I. Königl Ungar Geol Anstalt, Budapest 181 + xxv p

Valdes PJ, Scotese CR, Lunt DJ (2021) Deep ocean temperatures through time. Clim past 17:1483–1506. https://doi.org/10.5194/cp-17-1483-2021

van Hinsbergen DJJ, Torsvik TH, Schmid SM, Maţenco LC, Maffione M, Vissers RLM, Gürer D, Spakman W (2020) Orogenic architecture of the Mediterranean region and kinematic reconstruction of its tectonic evolution since the Triassic. Gondwana Res 81:79–229. https://doi.org/10.1016/j.gr.2019.07.009

Vickers ML, Bajnai D, Price GD, Linckens J, Fiebig J (2019) Southern high latitude warmth during the Jurassic-Cretaceous: new evidence from clumped isotope thermometry. Geol 47:724–728

Vickers ML, Fernandez A, Hesselbo SP, Price GD, Bernasconi SM, Lode S, Ullmann CV, Thibault N, Hougaard IW, Korte C (2020) Unravelling Middle to Late Jurassic palaeoceanographic and palaeoclimatic signals in the Hebrides Basin using belemnite clumped isotope thermometry. Earth Planet Sci Lett 546:116401. https://doi.org/10.1016/j.epsl.2020.116401

Vickers ML, Bernasconi SM, Ullmann CV, Lode S, Looser N, Morales LG, Price GD, Wilby PR, Hougård IW, Hesselbo SP, Korte C (2021) Marine temperatures underestimated for past greenhouse climate. Sci Rep 11:19109. https://doi.org/10.1038/s41598-021-98528-1

Vörös A (1993) Jurassic microplate movements and brachiopod migrations in the western part of the Tethys. Palaeogeogr Palaeoclimat Palaeoecol 100(1–2):125–145. https://doi.org/10.1016/0031-0182(93)90037-J

Weissert H, Mohr H (1996) Late Jurassic climate and its impact on carbon cycling. Palaeogeogr Palaeoclimat Palaeoecol 122(1–4):27–43. https://doi.org/10.1016/0031-0182(95)00088-7

Wierzbowski H, Bajnai D, Wacker U, Rogov MA, Fiebig J, Tesakova EM (2018) Clumped isotope record of salinity variations in the Subboreal Province at the Middle-Late Jurassic transition. Global Planet Change 167:172–189. https://doi.org/10.1016/j.gloplacha.2018.05.014

Yilmaz PO, Norton IO, Leary D, Chuchla RJ (1996) Tectonic evolution and paleogeography of Europe. In: Peri-Tethys Memoir 2:

Structure and prospects of Alpine basins and forelands, Ziegler PA, Horváth F (ed) Mém Mus Nat d'Hist Nat 170:47–60
Zuo F, Heimhofer U, Huck S, Adatte T, Erbacher J, Bodin S (2019) Climatic fluctuations and seasonality during the Kimmeridgian (Late Jurassic): stable isotope and clay mineralogical data from the Lower Saxony Basin, Northern Germany. Palaeogeogr Palaeoclimat Palaeoecol 517:1–15. https://doi.org/10.1016/j.palaeo.2018.12.018